AD-757 118

CARBON RESEARCH

Robert J. Akins, et al

Gulf Electronic Systems

Prepared for:

Advanced Research Projects Agency

31 January 1973

DISTRIBUTED BY:

NTIS

National Technical Information Service
U. S. DEPARTMENT OF COMMERCE
5285 Port Royal Road, Springfield Va. 22151

AD757118

GULF ELECTRONIC SYSTEMS

Gulf-EL-A12500

SEMIANNUAL TECHNICAL REPORT FOR THE PERIOD
JULY 1, 1972 TO DECEMBER 31, 1972

CARBON RESEARCH

Sponsored by
Advanced Research Projects Agency
Arlington, Virginia

ARPA Order No. 1861

January 31, 1973

DDC
RECEIVED
MAR 19 1973
B

R. J. Akins, J. L. Kaae, K. Koyama, R. J. Price, H. S. Shim,
and J. C. Bokros (P.I.) (714-299-2630)

GULF OIL CORPORATION
GULF ENERGY & ENVIRONMENTAL SYSTEMS COMPANY
San Diego, California 92112

Program Code Number:	1D10	Contract Date:	June 26, 1971
Contract Amount:	$226,235	Expiration Date:	June 25, 1973

This research was supported by the Advanced Research Projects Agency of the Department of Defense under Contract No. DAHC15-71-C-0282.

"The views and conclusions contained in this document are those of the authors and should not be interpreted as necessarily representing the official policies, either expressed or implied, of the Advanced Research Projects Agency or the U.S. Government."

Reproduced by
NATIONAL TECHNICAL
INFORMATION SERVICE
U S Department of Commerce
Springfield VA 22151

DISTRIBUTION STATEMENT A
Approved for public release;
Distribution Unlimited

Unclassified
Security Classification

DOCUMENT CONTROL DATA - R & D

(Security classification of title, body of abstract and indexing annotation must be entered when the overall report is classified)

1. ORIGINATING ACTIVITY *(Corporate author)*
Gulf Oil Corporation
Gulf Energy & Environmental Systems Company
P.O. Box 81608, San Diego, California 92138

2a. REPORT SECURITY CLASSIFICATION
Unclassified

2b. GROUP

3. REPORT TITLE
Carbon Research

4. DESCRIPTIVE NOTES *(Type of report and inclusive dates)*
Semiannual July 1, 1972 - December 31, 1972

5. AUTHOR(S) *(First name, middle initial, last name)*
Robert J. Akins, James L. Kaae, Karl (NMI) Koyama, Robert J. Price, Hong S. Shim, Jack C. Bokros

6. REPORT DATE	7a. TOTAL NO. OF PAGES	7b. NO. OF REFS
January 31, 1973	46	13

8a. CONTRACT OR GRANT NO	9a. ORIGINATOR'S REPORT NUMBER(S)
DAHC15-71-C-0282	Gulf-EL-A12500
b. PROJECT NO.	
c.	9b. OTHER REPORT NO(S) *(Any other numbers that may be assigned this report)*
d.	

10. DISTRIBUTION STATEMENT
Approved for public release; distribution unlimited.

11. SUPPLEMENTARY NOTES	12. SPONSORING MILITARY ACTIVITY
Details of illustrations in this document may be better studied on microfiche	Advanced Research Projects Agency Washington, D.C.

13. ABSTRACT

Additional codepositions of carbon (from propane) and silicon at temperatures near 1300°C suggest that the correlation between the carbon matrix density and the silicon concentration that has been observed is inherent in the deposition process. The carbon matrix density is independent of propane concentration and appears to be a unique function of the amount of silicon that is codeposited with the carbon. Accordingly, deposition of carbon-silicon alloys with both high silicon concentration and high carbon matrix density has not been possible. Future studies will involve deposition from methane.

Thin sections of glassy carbons, prepared by ion-sputtering, were examined using transmission electron microscopy. At low magnifications, a mosaic pattern is visible which has a configuration similar to the grain boundaries present in annealed metals. A uniform dispersion of spherical graphite inclusions approximately 0.1 to 0.4 μm in diameter was revealed with a concentration of about $0.01/\mu m^3$. The fine layer structure observable at 400,000X is similar to that reported previously for the pyrolytic carbons.

The thermal expansivities of the isotropic silicon-alloyed carbons have been determined. The expansivity decreases systematically with increasing silicon content, falling from $6.3 \times 10^{-6}\ °C^{-1}$ for material with 4 wt % silicon to $4.6 \times 10^{-6}\ °C^{-1}$ for material with 34 wt % silicon. The presence of silicon carbide reduces the thermal expansivity below that of

DD FORM 1 NOV 1473

Ia

Unclassified
Security Classification

14 KEY WORDS	LINK A		LINK B		LINK C	
	ROLE	WT	ROLE	WT	ROLE	WT
Pyrolytic carbons						
Fluidized beds						
Steady-state fluidized beds						
Chemical vapor deposition						
Pyrolytic-carbon wear properties						
Pyrolytic-carbon fatigue properties						
Pyrolytic-carbon strength properties						
Pyrolytic-carbon physical properties						
Silicon-alloyed pyrolytic carbons						

I b.

13. Abstract (Continued)

pure pyrocarbon with the same matrix density due to the low expansivity of the silicon carbide (4.6×10^{-6} °C^{-1}). The values lie between the bounds predicted by the zero stress model and the constant strain model.

The thermal conductivities of the silicon-alloyed carbons have been measured. The temperature dependencies are the same as those of the pure isotropic pyrolytic carbons, but the thermal conductivity of the silicon-alloyed carbon is consistently less than that of the pure carbons. It is concluded that the thermal conductivity of the silicon-alloyed carbon is controlled by the carbon phase and substitutionally dissolved silicon lowers the thermal conductivity below that of pure carbon.

Bending fatigue tests of glassy carbon show a behavior similar to that found for pure isotropic pyrolytic carbon. The endurance limit is very close to the single cycle fracture stress.

Wear tests have been extended and the data for the pure and alloyed carbons suggest that there are two wear mechanisms, one operative when the hardness of the abraded surface is less than about 200 DPH and the other operative when the hardness is greater. The wear caused by silicon-alloyed carbon disks is lowest for dense, pure carbon flats. Comparisons of the wear data and mechanical properties suggest that, for the carbons abraded by the silicon-alloyed disks, the wear rate correlates with the strain energy that can be accommodated by the abraded surface and is maximum for the dense, pure carbons.

SUMMARY

Additional codepositions of carbon (from propane) and silicon at temperatures near 1300°C suggest that the correlation between the carbon matrix density and the silicon concentration that has been observed is inherent in the deposition process. The carbon matrix density is independent of propane concentration and appears to be a unique function of the amount of silicon that is codeposited with the carbon. Accordingly, deposition of carbon-silicon alloys with both high silicon concentration and high carbon matrix density has not been possible. Future studies will involve deposition from methane.

Thin sections of glassy carbons, prepared by ion-sputtering, were examined using transmission electron microscopy. At low magnifications, a mosaic pattern is visible which has a configuration similar to the grain boundaries present in annealed metals. A uniform dispersion of spherical graphite inclusions approximately 0.1 to 0.4 μm in diameter was revealed with a concentration of about $0.01/\mu m^3$. The fine layer structure observable at 400,000X is similar to that reported previously for the pyrolytic carbons.

The thermal expansivities of the isotropic silicon-alloyed carbons have been determined. The expansivity decreases systematically with increasing silicon content, falling from $6.3 \times 10^{-6}\ °C^{-1}$ for material with 4 wt % silicon to $4.6 \times 10^{-6}\ °C^{-1}$ for material with 34 wt % silicon. The presence of silicon carbide reduces the thermal expansivity below that of pure pyrocarbon with the same matrix density due to the low expansivity of the silicon carbide ($4.6 \times 10^{-6}\ °C^{-1}$). The values lie between the bounds predicted by the zero stress model and the constant strain model.

The thermal conductivities of the silicon-alloyed carbons have been measured. The temperature dependencies are the same as those of the pure

isotropic pyrolytic carbons, but the thermal conductivity of the silicon-alloyed carbon is consistently less than that of the pure carbons. It is concluded that the thermal conductivity of the silicon-alloyed carbon is controlled by the carbon phase and substitutionally dissolved silicon lowers the thermal conductivity below that of pure carbon.

Bending fatigue tests of glassy carbon show a behavior similar to that found for pure isotropic pyrolytic carbon. The endurance limit is very close to the single cycle fracture stress.

Wear tests have been extended and the data for the pure and alloyed carbons suggest that there are two wear mechanisms, one operative when the hardness of the abraded surface is less than about 200 DPH and the other operative when the hardness is greater. The wear caused by silicon-alloyed carbon disks is lowest for dense, pure carbon flats. Comparisons of the wear data and mechanical properties suggest that, for the carbons abraded by the silicon-alloyed disks, the wear rate correlates with the strain energy that can be accommodated by the abraded surface and is maximum for the dense, pure carbons.

CONTENTS

FIGURES

FIGURES (continued)

FIGURES (continued)

TABLES

1. INTRODUCTION

The objective of the present program is to investigate the deposition process in steady-state fluid beds in order to gain a better understanding of the origin of the crystal structure and morphology of a wide range of isotropic pyrolytic carbons. Codeposited additives and catalysts are being used to increase the range of structures that are possible. The structures of the deposited carbons are being related to pyrolysis conditions, and variations in properties are being interpreted in terms of structure.

The statement of work is:

"a. Contractor shall use its best efforts to investigate the control of the structure of carbonaceous materials in the basic deposition process in fluid beds. Catalysts will be used to manipulate the deposition process and additives will be codeposited with the carbon to expand the number of structures attainable. The structure of the deposited carbon will be related to the deposition conditions and variations in properties will be interpreted in terms of the structure.

b. During the contract period 26 June 1971 through 25 June 1972, major emphasis will be devoted to investigating deposition in steady-state beds and characterizing the structures that are formed. The primary goal will be to develop an understanding of the deposition mechanisms and the structures formed so that the structure deposited may be controlled at will through appropriate adjustments of the pyrolysis conditions.

c. During the contract period 26 June 1972 through 25 June 1973, the investigation, detailed in b. above, shall be continued and using the information generated during this investigation study the relationship between the structure of the carbons formed and their properties."

This report presents the results obtained during the period 1 July 1972 to 31 December 1972 on Contract DAHC15-71-C-0282 (ARPA-1861). Two semiannual technical progress reports summarizing the work carried out on this contract have been issued, one for the period 1 July 1971 to 31 December 1971 (Report No. Gulf-E1-A10968 (Ref. 1) and the other for the period 1 January 1972 to 30 June 1972 (Report No. Gulf-E1-A12250) (Ref. 2).

2. DEPOSITION STUDIES

(R. J. Akins)

During the first year of this contract, a correlation between silicon concentration in codeposited silicon-carbon alloys and the carbon matrix density was found (Fig. 28 of Ref. 1). As the silicon concentration was increased (by reducing the propane concentration and increasing the flow of the helium carrier gas through the bubble contactor), the carbon matrix density of the deposits formed decreased, so that at 30 wt % silicon the matrix density was only 1.7 g/cm^3. Since it is well known that the mechanical properties are inferior for low-density carbons (Refs. 1, 3-5) and are enhanced by silicon additions (Ref. 6), it was desired to determine if silicon-carbon alloys could be deposited with both high carbon matrix density and high silicon content.

There are two possible explanations for the correlation described above. One explanation is that the presence of high chlorine and silicon concentrations in the gas alters the deposition mechanism so that the formation of low-density carbon is favored. The other is simply that when the CH_3SiCl_3 is added by passing the helium carrier gas through the bubbler contactor, a lesser amount of CH_3SiCl_3 is available for deposition when high propane concentrations are used, because the helium volume flow rate is proportionately lower and less CH_3SiCl_3 per mole of propane is introduced into the pyrolysis region. Since high density isotropic deposits are usually deposited with high hydrocarbon concentrations, the inability to deposit alloys with high carbon matrix density and high silicon concentrations may be an artifact of the process.

The above facts suggest that the desired deposits (high-density carbon-silicon alloys) might be attained by revising the deposition process so that larger CH_3SiCl_3 flow rates can be introduced when high propane concentrations are used in the deposition. Accordingly, during the past six months, a new

injection system was developed which allows the methyltrichlorosilane (MTS) injection rate to be independent of the helium and propane flow rates. The new system is shown schematically in Fig. 1.

A series of deposition runs were carried out using the new apparatus in an attempt to produce silicon-carbon alloys with high carbon matrix densities together with high silicon concentrations. The conditions used in the depositions are listed in Table 1. The parameters that characterize the deposits formed are listed in Table 2.

The deposit made at 1350°C and 1948 cm^3/min MTS flow was low in silicon content (8.5%). A second run at a lower temperature resulted in a slightly higher silicon content (17%). Finally, using a slightly higher temperature, (approximately 1300°C), a deposit with 31 wt % silicon was formed. Analysis of the deposit showed that the carbon matrix density was only 1.71 g/cm^3, i.e., almost exactly that predicted by the plot of carbon matrix density versus silicon concentration that was reported previously (Fig. 2).

The results in Fig. 2 show that the secondary correlation between propane concentration and the carbon matrix density is an artifact, and indicates further that the correlation between carbon matrix density and silicon concentration is probably due to a basic change in the pyrolysis mechanism caused by the presence of high silicon and/or chlorine concentrations in the pyrolysis chamber.

The new data points from Table 2, when plotted on Fig. 7 of Ref. 2, provide further information about the dependence of the hardness on silicon concentration, carbon matrix density, the L_c parameter, and the deposition conditions. The new data show that the correlation between propane concentration and hardness evident on Fig. 7 of Ref. 2 is fortuitous. The carbons formed with the new injector pump, using 60% propane, lie in the 7% and 25% ranges indicated on the plot. The data substantiate that hardness increases with increasing density and silicon concentration, and decreases with an increasing L_c parameter.

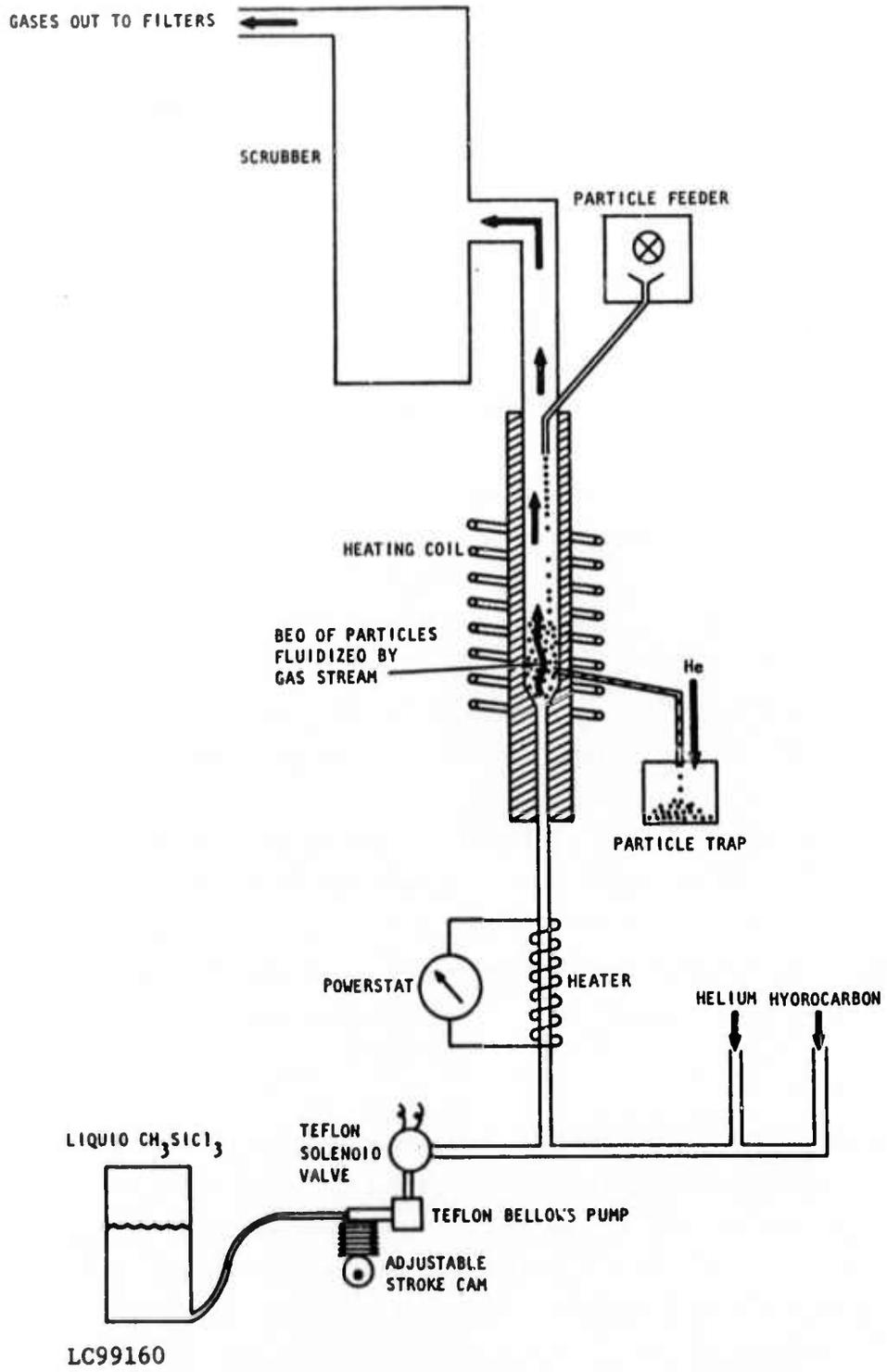

Fig. 1. Schematic diagram of steady-state fluidized bed equipped with pump injector system.

TABLE 1

DEPOSITION CONDITIONS FOR CODEPOSITING CARBON-SILICON ALLOYS DEPOSITED IN STEADY-STATE BEDS USING PROPANE AND METHYLTRICHLOROSILANE[a]

Run Number	C_3H_8 Concentration (%)	Control Temperature (°C)[b]	Bed Temperature (°C)	CH_3SiCl_3 Vol. Flow (RT) (cm^3/min)	Carbon Deposition Efficiency (%)	Silicon Deposition Efficiency (%)	Average Deposition Rate (μm/min)	Coating Thickness (in.)
5638-49	60	1350	1240	1948	48.8	6.7	4.65	.011
5638-53	60	1200	∿1000	5844[c]	27.3	2.8	2.90	.007
5638-51	60	1400	∿1300	5844[c]	40.5	10.0	6.17	.009

[a] Total flow rate was 18 l/min (C_3H_8 and He) at room temperature. Methyltrichlorosilane was injected through a bellows pump. Short coater design was used based on the data reported in Ref. 1.

[b] Extrapolated from Fig. 3, Ref. 1.

[c] 38.3 g/min.

TABLE 2

STRUCTURAL DATA FOR CODEPOSITED CARBON-SILICON DEPOSITS FORMED IN FLUIDIZED BEDS USING PROPANE AND METHYLTRICHLOROSILANE INJECTED AT HIGH FLOW RATES

Run Number	C_3H_8 Concentration (%)	Control Temperature (°C)	Bed Temperature (°C)[a]	Silicon Content (wt %)	Microhardness (DPH at 50 g load)	Deposit Density (g/cm^3)	Calculated Carbon Matrix Density (g/cm^3)	Apparent Crystallite Height (Å)
5638-49	60	1350	1240	8.5	290	(b)	(b)	(b)
5638-53	60	1200	∿1000	17.0	412	2.073	1.86	20
5638-51	60	1400	∿1300	31.0	378	2.156	1.71	31

[a] Extrapolated from Fig. 3 of Ref. 1.

[b] Not determined.

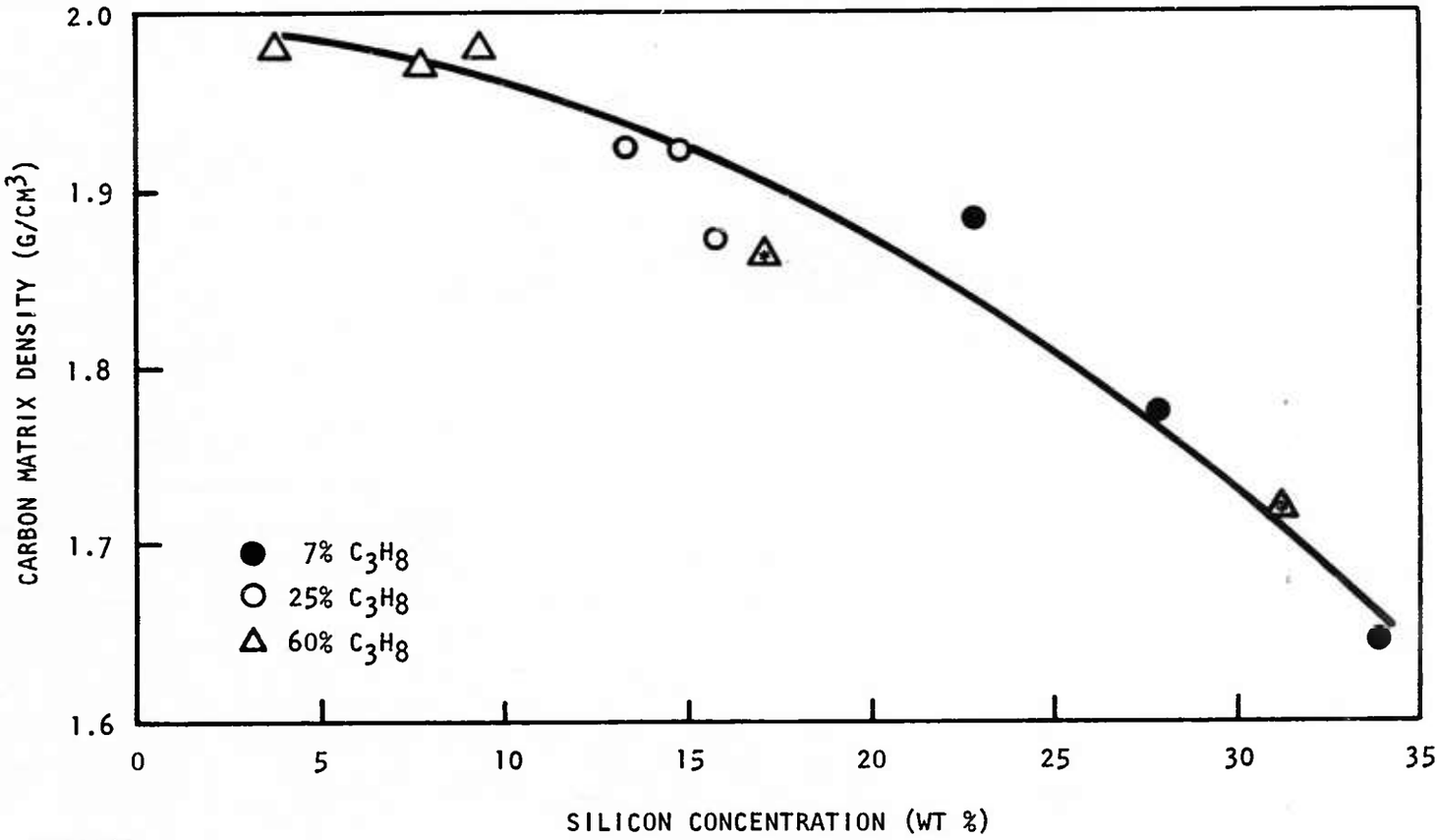

Fig. 2. Carbon matrix density versus silicon concentration for carbon-silicon materials deposited at temperatures in the range 1200° to 1400°C from 7%, 25%, and 60% propane with CH_3SiCl_3 additive. The two asterisked triangular points for 60% propane are for deposits formed using the new pump injector system.

It is worth noting that the microstructure of the carbons deposited with the new system is more uniform and has fewer soot inclusions than those deposited previously (Figs. B-19 and B-20 of Ref. 1). The microstructure of the deposit formed in run 5638-51 is shown in Fig. 3. The mechanical properties of this deposit will be determined in the next contract period.

In future deposition studies, attention will be shifted to studies of the deposition of pure and alloyed isotropic carbons from methane at temperatures below approximately 1400°C.

The findings of the studies of pure and alloyed isotropic carbons deposited from propane will be presented at the 11th Conference on Carbon and submitted to Carbon for publication. The abstract of this paper, "The Deposition of Pure and Alloyed Isotropic Carbons in Steady-State Fluidized Beds," by R. J. Akins and J. C. Bokros, follows:

"Pure and alloyed isotropic carbons have been deposited in steady-state fluidized beds using a wide range of deposition conditions. The results have shown that in the pure carbon system, the structure, as measured by density, L_c parameter, and anisotropy, can be easily controlled by adjusting the deposition parameters. At the same low deposition temperatures, the L_c parameter increases with propane concentration. The L_c parameters and density both decrease with increasing deposition temperature. The hardness values were found to increase with density and decrease with increasing L_c parameter. Codeposition of silicon in the presence of chlorine increases the hardness of the carbons and modifies the deposition process. The carbon matrix density decreased with increasing deposition temperatures only at low propane concentrations, while the L_c parameter increased over the same temperature range. Codeposition of boron in the presence of chlorine resulted in carbons that were relatively soft and have large L_c parameters."

K99059 200X

Fig. 3. Microstructure of deposit 5638-51 made with high C_3H_8 concentration and high methyltrichlorosilane flow.

3. STRUCTURAL STUDIES

(J. L. Kaae)

During this period, glassy carbon was thinned by ion sputtering and examined by transmission electron microscopy in order to compare the microstructure of this carbon with those reported previously for pyrolytic carbons. Descriptions of the microstructures of glassy carbon that have been published (Ref. 8) were derived from small chips obtained by fragmentation. The areas examined were small and observations were confined to layer-plane arrangements. Ion sputtering produces thinning of much larger regions than fragmentation, and allows examination of the microstructure on a broader scale. As a result, several new structural features have been revealed.

The glassy carbon which was examined was obtained from the Beckwith Carbon Company and carried the designation 1800 grade. The specimen was first thinned, by mechanical polishing, to a thickness of 0.001 in. and then bombarded by argon ions until it was sufficiently thin for transmission of electrons.

The mosaic pattern in Fig. 4 is caused by a network in which transmission by the electrons is easy. Detailed examination of the regions making up the mosaic pattern suggest that the effect was due to differences in the thickness of the thin section. The mosaic pattern is apparently due to selective thinning, which may reflect a subtle structural difference between the two regions. Additional glassy carbon specimens will be thinned using a variety of different conditions to see how the mosaic pattern depends on thinning conditions.

In addition to the mosaic pattern, many small spherical inclusions were revealed (Fig. 5). Selected area diffraction from a small region containing the inclusion indicates that the features are graphitic particles. Many of the spots produced by the inclusion in selected area diffraction (Fig. 6) fall on the diffraction rings produced by the glassy carbon.

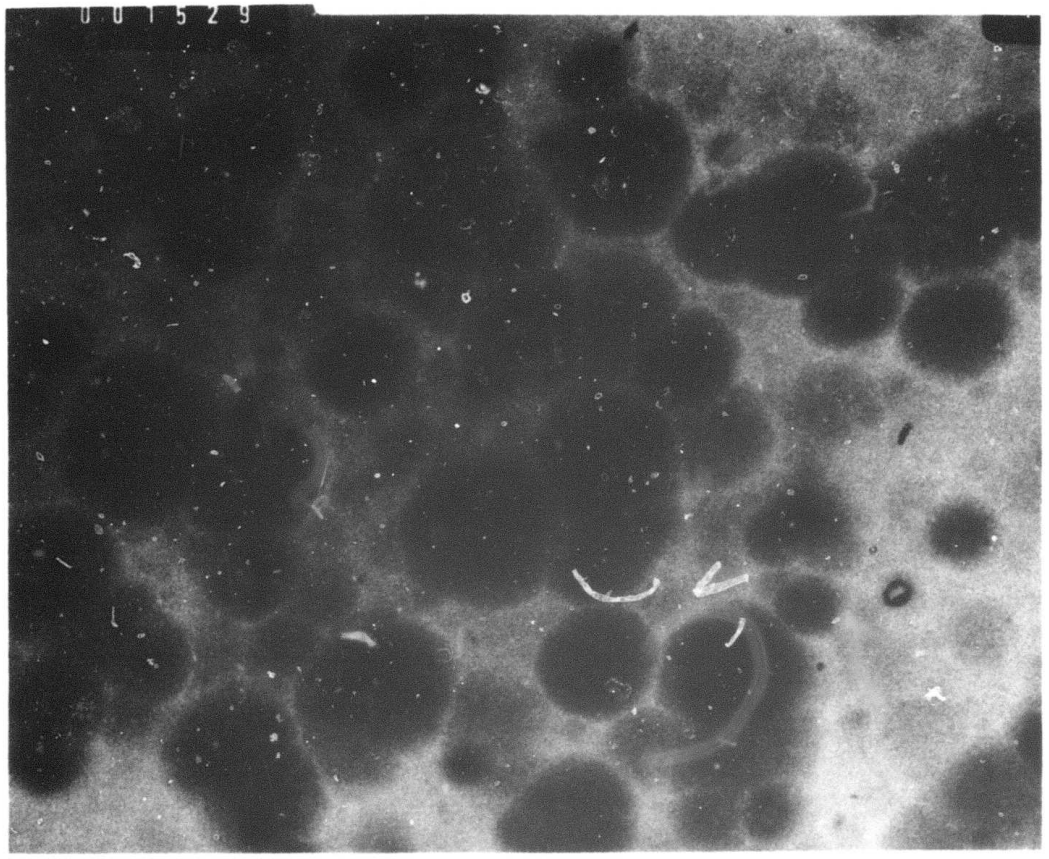

K99057 9500X

Fig. 4. Transmission electron micrograph of glassy carbon showing mosaic pattern and small spherical inclusions.

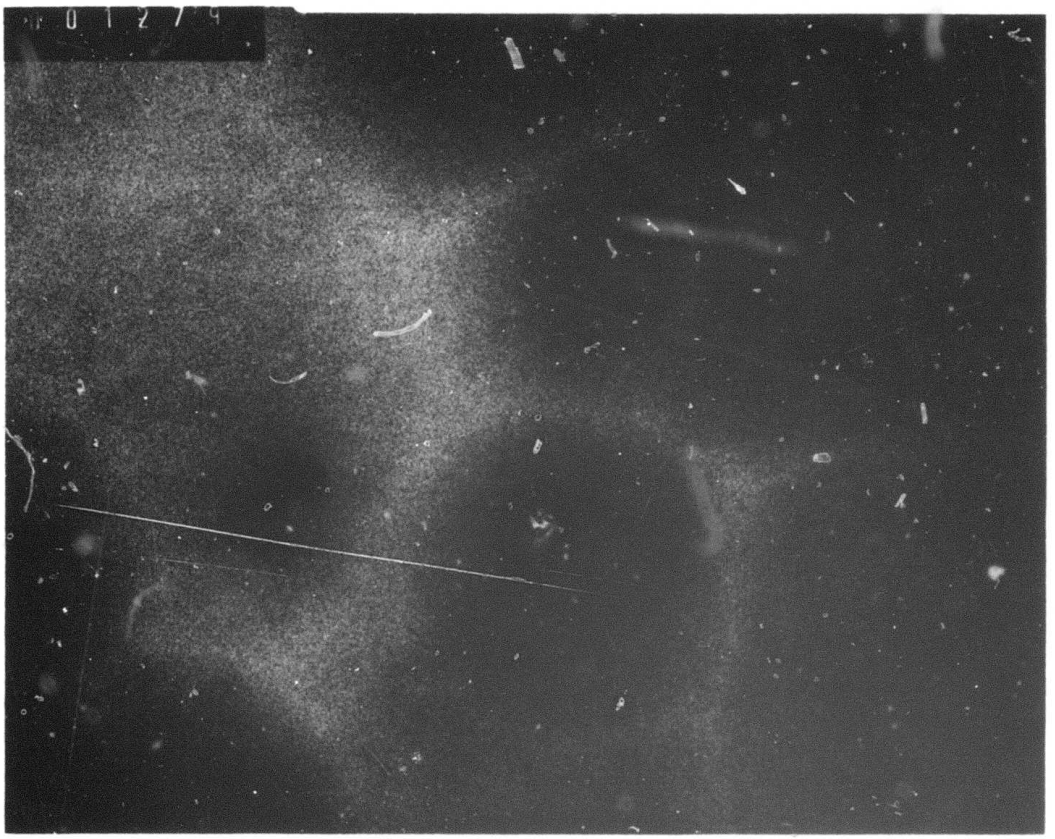

K99055 40,000X

Fig. 5. Small spherical inclusion in glassy carbon.

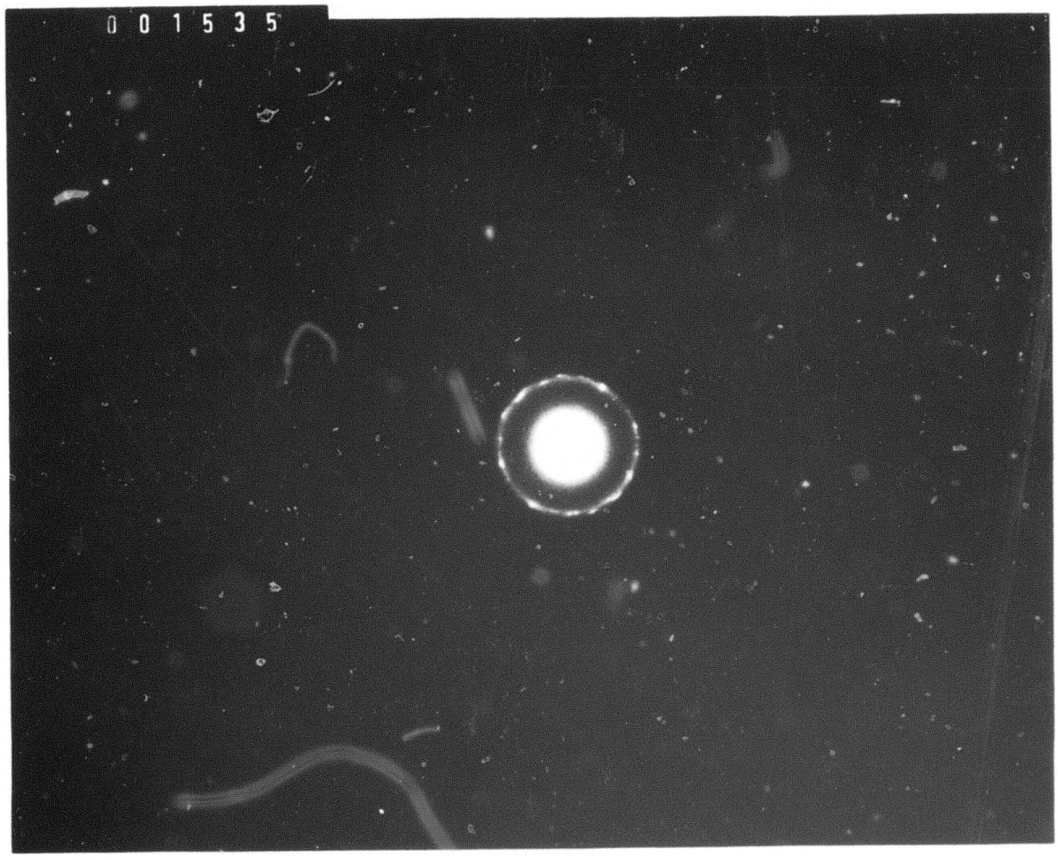

K99053

Fig. 6. Selected area diffraction pattern from region containing an inclusion. Spots have been indexed as (002), (100), (101), (004), (103), and (110) of graphite.

The high-magnification micrograph shown in Fig. 7 shows the abrupt transition from the ordered structure of the inclusion to the disordered structure of glassy carbon. The inclusions ranged in size from 0.1 μm to 0.4 μm, with a density of approximately $2 \times 10^5/cm^2$. If one assumes that the particles are large compared to the thickness of the section, the volume density is approximately $0.01/\mu m^3$. These regions could influence the mechanical properties by acting as fracture initiation sites and their removal could lead to an increase in the fracture strength.

The source of the graphitized regions is open to speculation. One possibility is that they are associated with noncarbonaceous particles which give rise to local graphitization, either through a differential thermal expansion stress-induced effort or through a catalytic effect. It does not seem likely that the graphite inclusions were formed from stress-induced graphitization around a gas bubble, since the gas most likely present during carbonization would be hydrogen, which diffuses rapidly and is lost at high temperature.

The structure of glassy carbon at high magnification (Fig. 8) is similar to the structure observed by Ban and Hess (Ref. 8) except that in the present case the foil was too thick for phase-contrast effects, so that it was not possible to resolve layer planes; small packets however can be observed in many areas (indicated by arrows on Fig. 8). Comparison of the fine microstructure of glassy carbon with the fine microstructure of low-density isotropic pyrolytic carbons deposited at 1450°C (Fig. 9) shows that the fine structure of the two materials is very similar. The only difference is that the structure of the low-density pyrolytic carbon is coarser. The fine microstructural features of low-density pyrolytic carbons deposited at 1650°C are coarser than those shown in Fig. 9, but in other respects are similar to those of glassy carbon.

The results of the structural studies of pyrolytic and glassy carbons will be presented at the 11th Conference on Carbon and submitted for publication in Carbon. The abstract of this paper, "Morphology of Growth Features in Isotropic Pyrolytic Carbons Deposited Below 1500°C," by J. L. Kaae, follows:

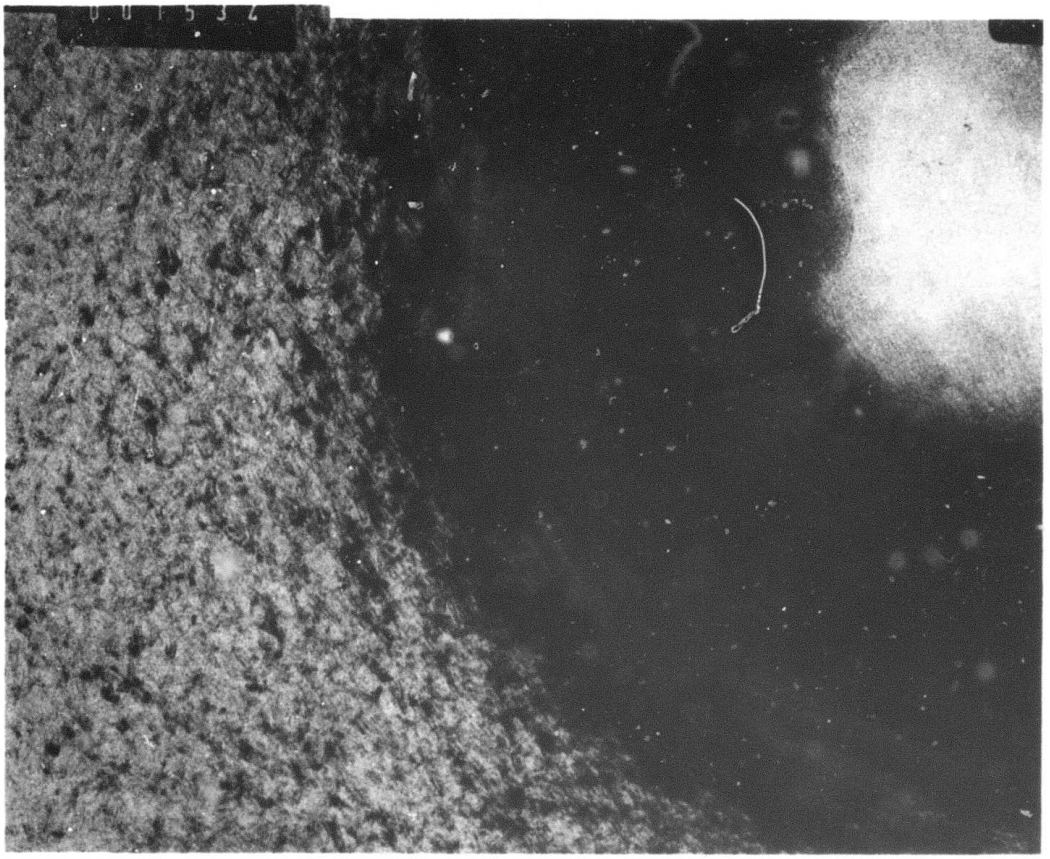

K99054 440,000X

Fig. 7. Region of transition from the graphitic structure of the inclusion to the disordered structure of the glassy carbon.

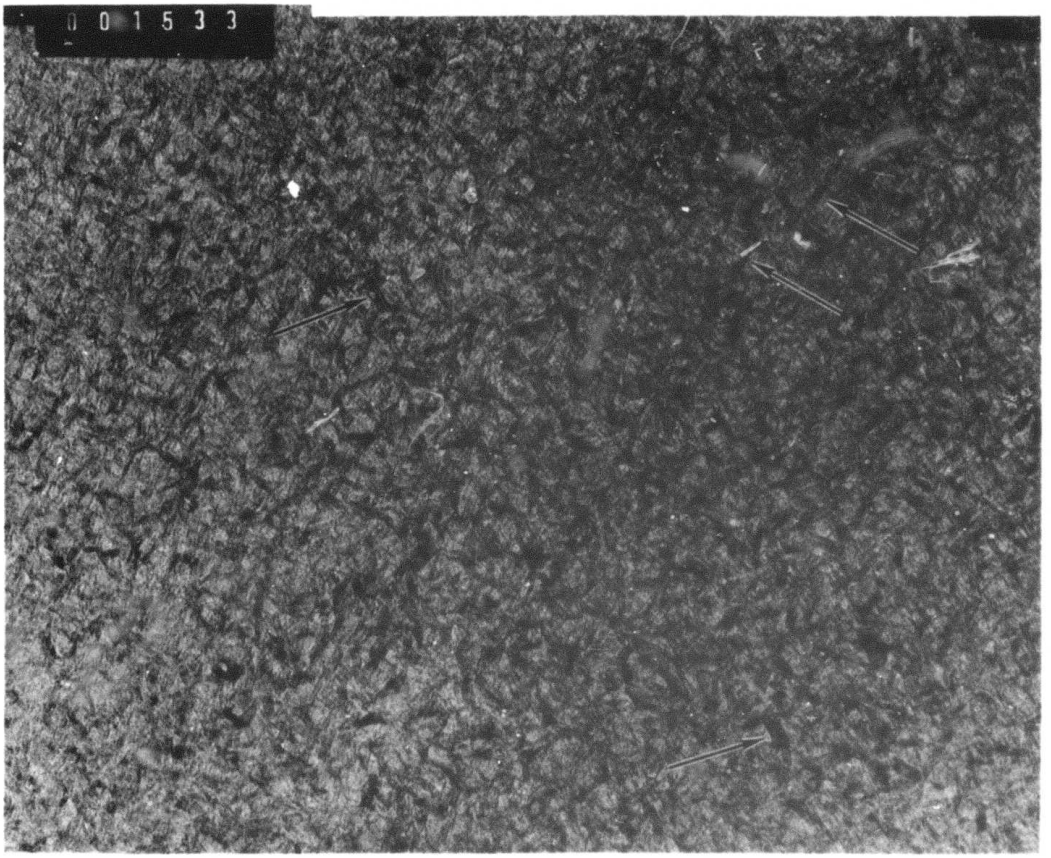

K99056 440,000X

Fig. 8. Fine microstructure of the glassy carbon. Packets of layer planes are indicated by arrows.

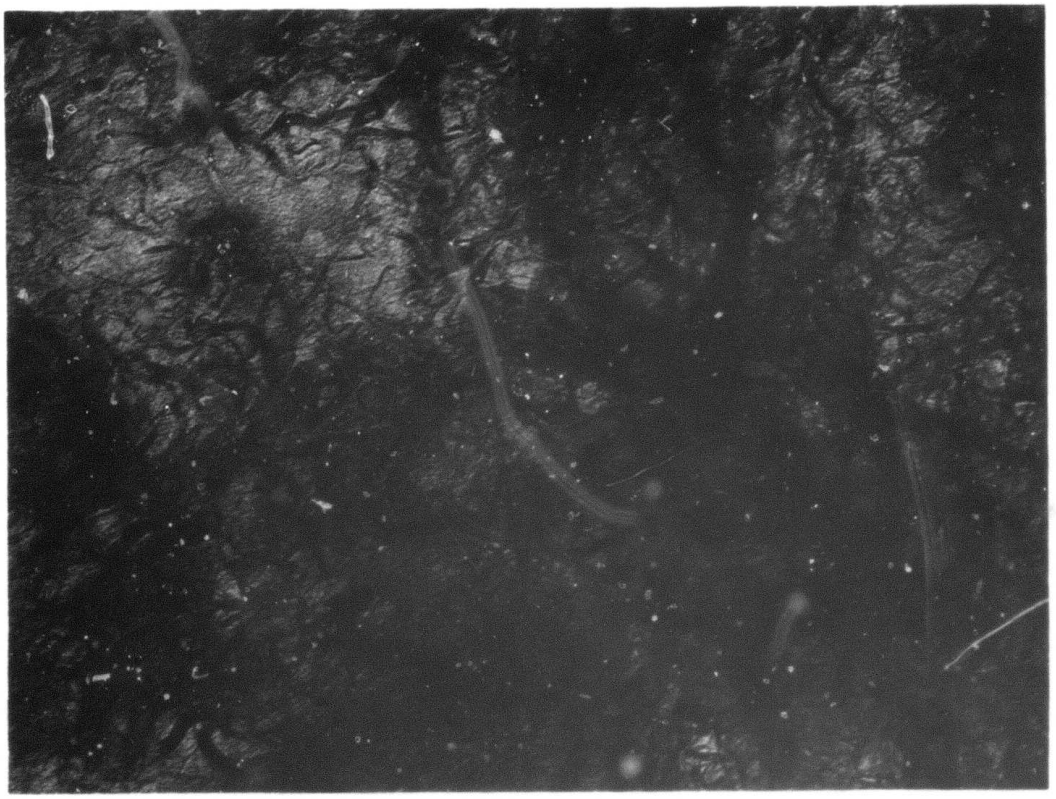

K99058 44,000X

Fig. 9. Fine microstructure of a low-density pyrolytic carbon.

"Pure and alloyed isotropic pyrolytic carbons deposited in the temperature range 1450°C to 1250°C from the decomposition of propane were thinned by ion sputtering and examined by transmission electron microscopy. A variety of structural features were observed and related to the origin of the carbon. Features were observed that appeared to have formed in the gas phase and acted as droplet nuclei. Others appeared to have formed by subsequent growth. The structures of the pyrolytic carbons are compared with the structure of a glassy carbon."

4. PHYSICAL PROPERTIES

(K. Koyama and R. J. Price)

4.1. THERMAL EXPANSIVITY OF SILICON-ALLOYED PYROLYTIC CARBONS

The techniques and results of measurements of the thermal expansivity of isotropic pyrolytic carbons were described in the two previous reports in this series (Refs. 1, 2). Similar measurements have now been made on a series of silicon-alloyed pyrolytic carbons. The expansivity of strips was measured parallel to the deposition plane using a silica dilatometer. Measurements were made between room temperature and 1000°C.

Deposition conditions for the silicon-alloyed carbons are given in Table 4 of Ref. 2. The thermal expansion curves were similar in shape to those of pure pyrolytic carbons, with a small amount of upwards curvature (Ref. 1). The mean thermal expansivity between room temperature and 1000°C is listed in Table 3 and plotted as a function of silicon content in Fig. 10. The thermal expansivity decreases systematically with increasing silicon content, falling from 6.3×10^{-6} $°C^{-1}$ for material with 4 wt % silicon to 4.6×10^{-6} $°C^{-1}$ for material with 34 wt % silicon. A portion of this decrease is attributable to the decrease in the matrix carbon density as the silicon content increases. The matrix carbon densities are indicated in Fig. 10, and the thermal expansivities of pure carbons with the same density (from Ref. 2) are plotted as solid points on the same figure.

The data in Fig. 10 show that the presence of silicon carbide reduces the thermal expansivity of the composite below that of pure pyrocarbon with the same density as the carbon matrix of the composite. This results from the low expansivity of silicon carbide (4.6×10^{-6} $°C^{-1}$) compared with the pyrocarbon matrix.

TABLE 3

THERMAL EXPANSIVITY AND THERMAL CONDUCTIVITY OF SILICON-ALLOYED PYROLYTIC CARBONS

Deposition Run No.	Properties			Thermal Expansivity Run Number	Mean Thermal Expansivity 22° - 1000°C x 10^6 ($°C^{-1}$)	Thermal Conductivity Run Number	Thermal Conductivity (cal/cm-sec-°C)				
	Silicon Content (wt %)	Carbon Density (g/cm^3)	Apparent Crystallite Height, L_c (Å)				22°C	200°C	400°C	600°C	800°C
5408-67	4.0	1.98	48	K0308	6.32	K0299	0.0127	0.0160	0.0185	0.0190	0.0186
5408-65	8.0	1.97	32	K0444	5.97	K0448	0.0066	0.0081	0.0091	0.0097	0.0101
5408-57	9.5	1.98	39	K0306	6.38	K0297	0.0088	0.0117	0.0130	0.0136	--
5408-83	13.5	1.92	48	K0445	5.54	K0449	0.0104	0.0125	0.0125	0.0137	0.0135
5408-69	15.0	1.92	35	K0309	5.41	K0300	0.0050	0.0067	0.0075	0.0085	0.0088
5408-59	16.0	1.87	40	K0443	5.35	K0447	0.0095	0.0112	0.0122	0.0132	0.0141
5408-87	23.0	1.88	35	K0310	4.87	K0301	0.0067	0.0087	0.0095	0.0099	0.0100
5408-61	28.0	1.77	38	K0307	4.78	K0298	0.0073	0.0086	0.0100	0.0102	0.0099
5408-85	34.0	1.64	38	K0446	4.53	K0450	0.0076	0.0095	0.0106	0.0107	0.0112

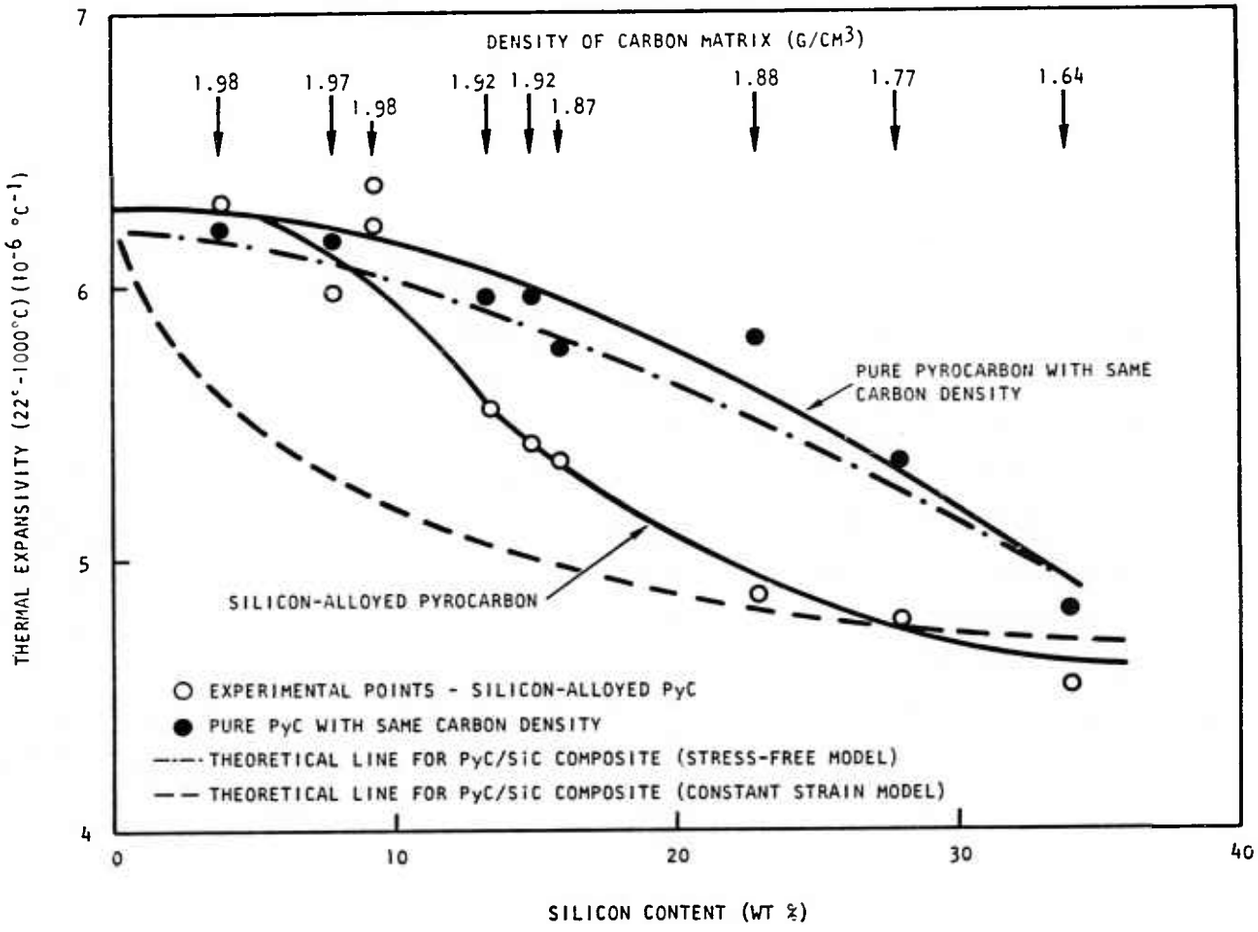

LC99161

Fig. 10. Thermal expansivity of silicon-alloyed pyrocarbons as a function of silicon content.

If there were no elastic interaction between the phases, the thermal expansivity of a two-phase composite, α_c, would be given by a rule-of-mixtures formula:

$$\alpha_c = \sum_i \alpha_i V_i \quad , \tag{1}$$

where α_i and V_i are the thermal expansivity and volume fraction of the i^{th} phase. In the presence of elastic interactions which force the aggregate to expand with a uniform strain, the expansivity of the composite would be given by:

$$\alpha_c = \frac{\sum_i \alpha_i V_i K_i}{\sum_i V_i K_i} \quad ,$$

where K_i is the bulk elastic modulus of the i^{th} phase. If both phases have the same Poisson's ratio, Young's modulus, E_i, may be substituted for K_i:

$$\alpha_c = \frac{\sum_i \alpha_i V_i E_i}{\sum_i V_i E_i} \quad . \tag{2}$$

For the composite body to have minimum strain energy, the actual thermal expansivity should be between the two bounds given by Eq. 1 (zero stress model) and Eq. 2 (constant strain model).

Lines representing Eqs. 1 and 2 are shown in Fig. 10. Appropriate values for the thermal expansivity and Young's modulus of the carbon phase were taken from Refs. 1 and 2. A thermal expansivity of 4.6×10^{-6} °C^{-1} and a Young's modulus of 62×10^6 psi (4.3×10^5 MN/m^2) were assumed for silicon carbide. It may be seen that the experimental points fall between the bounds representing the zero stress model (Eq. 1) and the constant strain model (Eq. 2), as expected. For low silicon contents, where the silicon carbide is in the form of finely dispersed particles, the expansivities are close to the upper (zero stress) bound, representing the case where the carbon matrix dominates the expansion behavior. For high silicon contents, where the silicon

carbide consists of platelets, the values are closer to the lower (constant strain) bound. This may be explained by the platelet morphology causing the high-elastic-modulus silicon carbide to dominate expansion behavior.

4.2. THERMAL CONDUCTIVITY OF SILICON-ALLOYED PYROLYTIC CARBONS

Preliminary measurements of the thermal conductivity of silicon-alloyed pyrocarbons were given in the previous report in this series (Ref. 2). Further measurements have now been made. The carbons were prepared in the form of disks approximately 7 mm in diameter and 0.3 mm thick, and the thermal diffusivity was measured by the heat-pulse method. The thermal conductivity was obtained by multiplying the thermal diffusivity by the density and the heat capacity, calculating the heat capacity from the weight fractions of silicon carbide and pyrocarbon. The heat capacities of the two phases were taken from the literature, assuming that recent values for glassy carbon (Ref. 9) apply to pyrocarbon.

The full results are tabulated in Table 3. The room temperature thermal conductivity for both pure pyrocarbons and silicon-alloyed pyrocarbons is plotted as a function of apparent crystallite height, L_c, in Fig. 11. The full results confirm the preliminary measurements reported previously. The temperature dependence curve of the thermal conductivity of the silicon-alloyed carbons is consistently less than that of pure pyrocarbon with the same L_c. The data on silicon-alloyed carbons all lie in one scatter band, showing no correlation between thermal conductivity and silicon content.

The conclusions from this work remain the same as the preliminary conclusions reached in the previous report (Ref. 2). The thermal conductivity of the silicon-alloyed carbons is evidently controlled by the carbon phase, and substitutionally dissolved silicon lowers the thermal conductivity substantially below that of pure pyrocarbon.

A summary of the results of the studies of the thermal expansivity and thermal diffusivity of pure and silicon-alloyed isotropic pyrolytic carbons

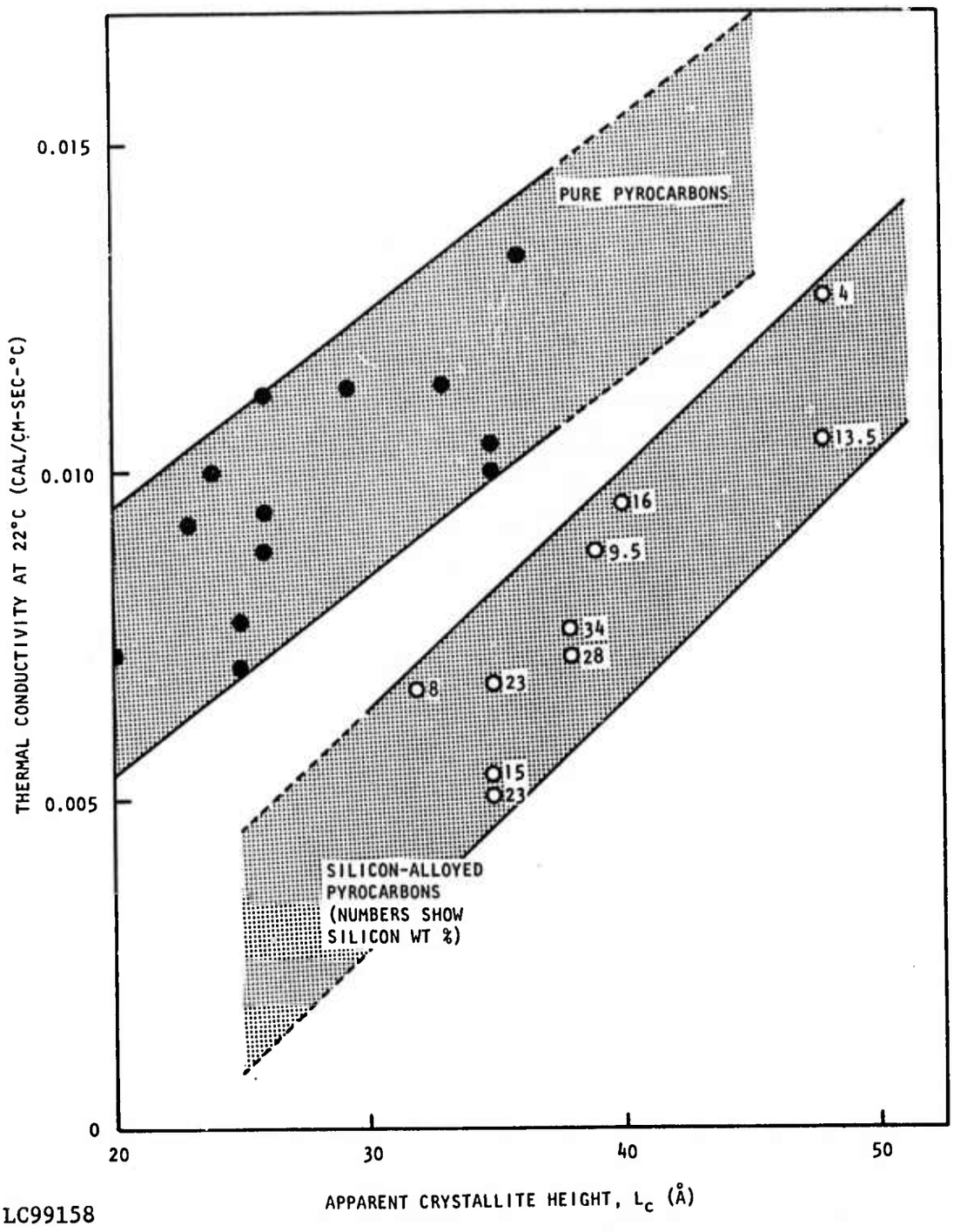

Fig. 11. Thermal conductivity at 22°C of pure pyrocarbons (closed points) and silicon-alloyed pyrocarbons (open points) as a function of apparent crystallite height (L_c).

will be presented at the 11th Conference on Carbon and submitted to Carbon for publication. The abstract of this paper, "Thermal Expansivity and Thermal Diffusivity of Silicon-Alloyed Pyrocarbons," by R. J. Price and K. Koyama, follows:

"Measurements were made of the thermal expansivity and thermal diffusivity of isotropic fluidized-bed pyrocarbons containing up to 34 wt-% silicon. The thermal expansivities decreased with increasing silicon content and agreed with the expected values for silicon carbide-pyrocarbon composites. The thermal conductivities of the silicon-alloyed carbons were consistently lower than those of pure pyrocarbons with similar apparent crystallite heights (L_c), suggesting that substitutionally dissolved silicon reduces the conductivity of the carbon matrix."

5. MECHANICAL PROPERTIES

5.1. FATIGUE (H. S. Shim)

The apparatus used for measuring the fatigue strength of pyrolytic carbons has been improved. In the past, the motor that actuates the knife edge started when it and the specimen were brought into contact. As a result, the deflection experienced by the specimen in the first few cycles often exceeded the desired value, and sometimes caused premature fracture. In the new procedure, the specimen and knife edge are brought into contact gradually while the knife edge is in motion at 60 cpm. After complete contact is achieved, the cycle rate is increased to the value desired (1700 cpm).

Using the new procedure, the deflection versus cycles to failure was measured (Fig. 12) for glassy carbon (ρ = 1.50 g/cm^3, 149 DPH). When Young's modulus is available, the deflection data in Fig. 12 can be converted to stress. The data indicate that, like isotropic pyrolytic carbons, the fatigue limit of glassy carbon is equal to the single cycle fracture stress; i.e., there is no dynamic effect. This behavior may have been expected for purely crystalline carbons since dislocations, if they exist in the material, are immobile (Refs. 10, 11). It is worth noting that the endurance limit of graphitic materials has been reported to be approximately 50% of the single cycle fracture stress (Refs. 12, 13).

5.2. WEAR (H. S. Shim, J. L. Kaae)

During the past contract period, considerable new data have been obtained that relate the wear caused by a radiused, polished disk rubbing on a polished, flat plate. The apparatus and procedure have been described in Ref. 1. The data are for a 2.2 g bearing load and a speed of 60 rpm in water. The identification codes for the materials are related in Table 4.

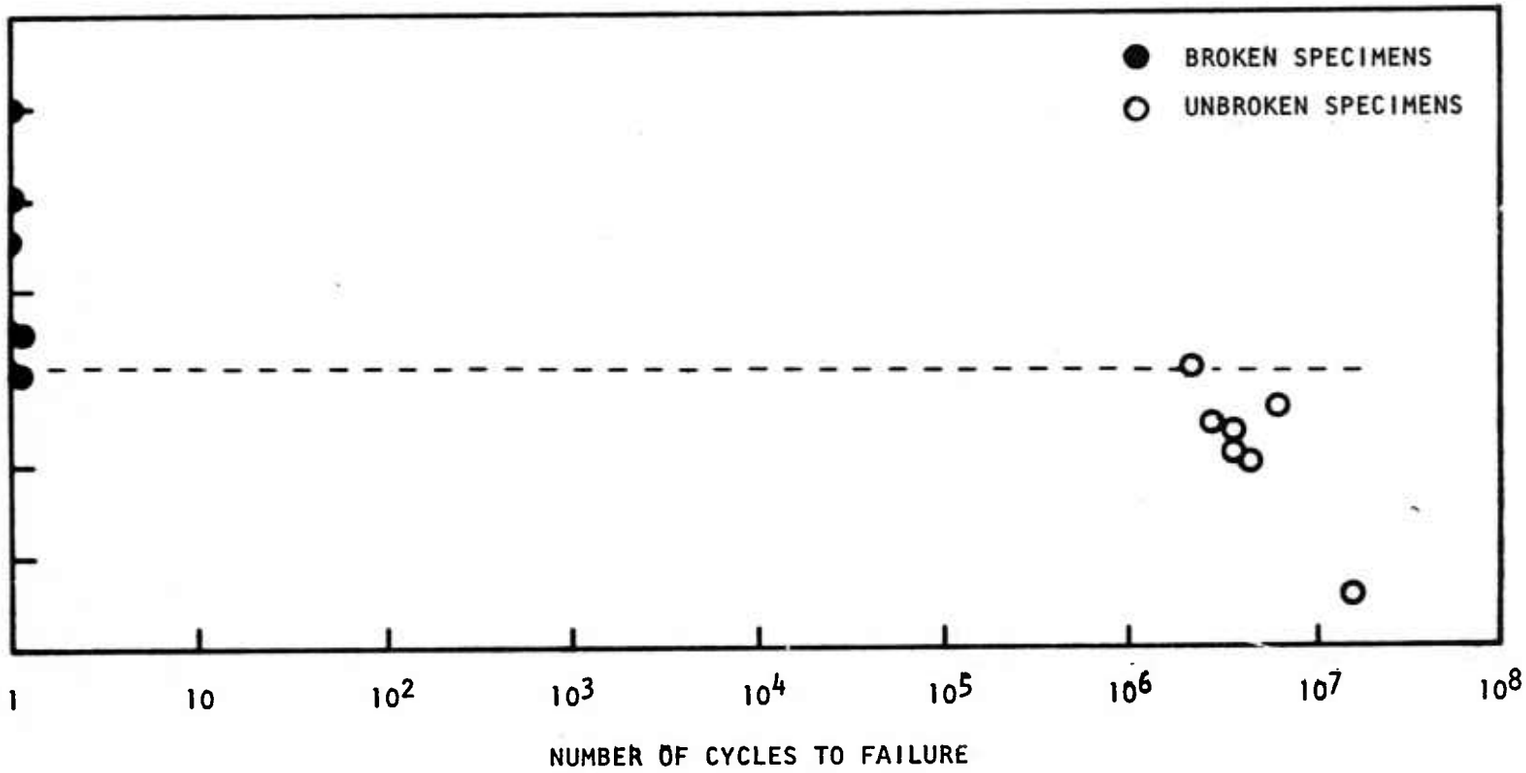

LC99159

Fig. 12. Deflection in cantilever bending versus cycles to failure for glassy carbon (ρ = 1.50 g/cm^3, 149 DPH).

TABLE 4

FLAT IDENTIFICATION NUMBERS AND COMPOSITIONS

Identification Number	Flat	Silicon-Carbon (wt %)	Hardness Number (DPH at 50 g load)	Carbon-Matrix Density (g/cm^3)	L_c Parameter (Å)
1	5408-17	0	153	1.46	20
2	5408-5	0	210	1.78	30
3	5408-7	0	219	1.97	36
4	5408-65	8	295	1.97	32
5	5408-69	15	352	1.92	48
6	5408-59	16	212	1.87	40
7	5408-87	23	430	1.88	35
8	Titanium	(a)	--	(a)	(a)
9	Stellite 21	(a)	--	(a)	(a)
10	Glassy Carbon	0	149	1.50	20
11	17C14	8.5	309	--	--

(a) Does not apply

5.2.1. Wear Caused by Pure Carbon Disks Rubbing on Various Carbon and Metal Flats

The data in Fig. 13 are for a dense, pure carbon disk (ρ = 1.97 g/cm^3, 219 DPH) rubbing on the flats listed in Table 4. For the pure carbons (No. 1, 2, 3, and 10 in Table 4), the wear rates caused by the disk increase in the order of their hardness; the carbon flats alloyed with silicon (No. 4, 5, 6, 7, and 11) experience less wear than the pure carbons. The most wear resistant carbon alloy (No. 4) has an intermediate hardness (295 DPH), the lowest silicon content, and the highest carbon matrix density. The wear rates for the alloyed carbon flats are in the order of the carbon matrix density and there is no clear correlation with silicon content or hardness.

The wear caused by the dense carbon disk on a Stellite 21 flat is low and comparable with that for the silicon alloyed materials. The wear rate of the titanium flat is higher than that experienced by the alloyed carbon and Stellite 21 but lower than that of pure carbons.

The data in Fig. 14 are for a pure carbon disk with a moderate density (1.8 g/cm^3, 210 DPH) rubbing on the flats listed in Table 4. The relative wear rates are nearly the same as those for the previous case except the order of the wear resistance among the alloyed carbons has changed and all the corresponding rates are lower than those in Fig. 13.

The data in Fig. 15 are for a pure carbon disk with a low density (1.46 g/cm^3) and hardness (153 DPH) rubbing on the flats listed in Table 4. The relative rates remain nearly the same as those in Figs. 13 and 14. The wear rates for the pure carbons decrease as their density and hardness increase; the wear resistance of the silicon-alloyed carbons is superior. In all cases, the Stellite 21 flats wear less than titanium when abraded by pure carbon disks.

It is interesting to note that the wear resistance of mechanically polished titanium is the same as that of electrochemically polished titanium.

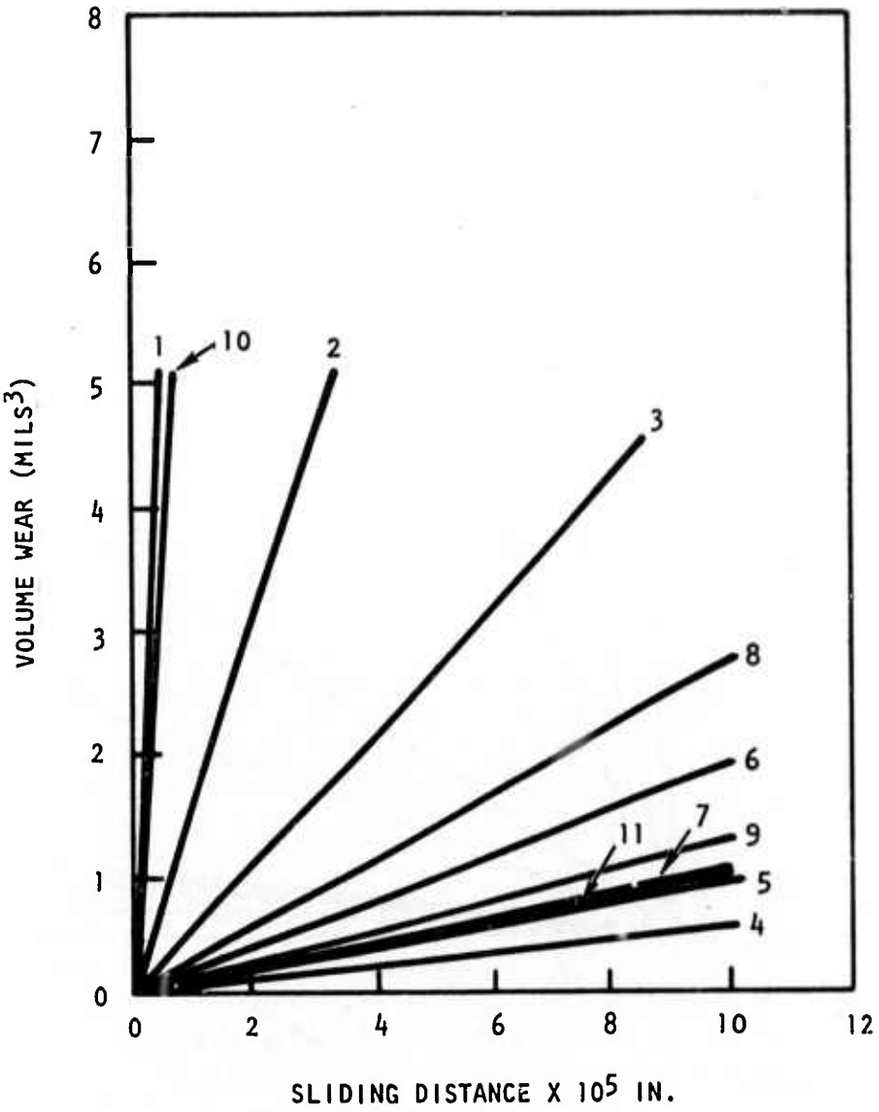

LC99164

Fig. 13. Wear caused by a dense (1.97 g/cm^3) pure carbon disk (219 DPH) rubbing on various flats. (The identification numbers of the flats are listed in Table 4.) Conditions: 2.2 g load and 60 rpm in water.

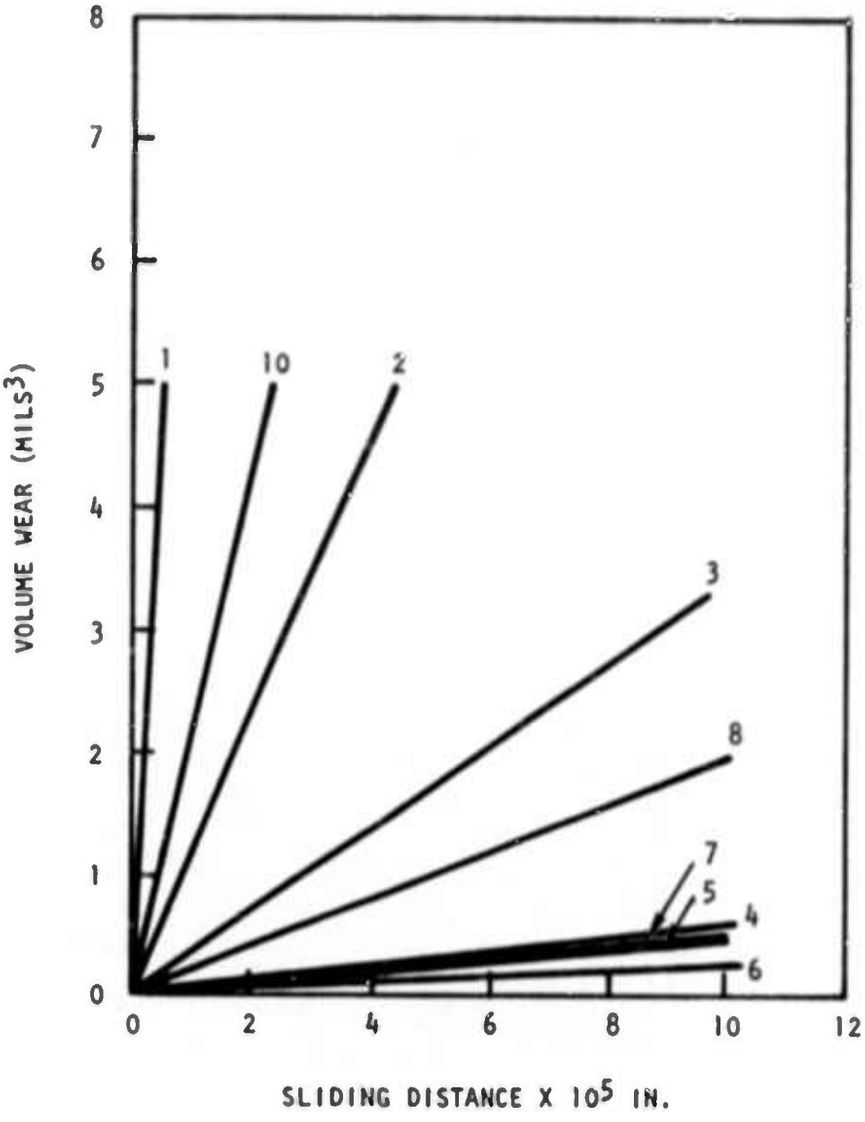

LC99165

Fig. 14. Wear caused by a pure carbon disk with moderate density (1.78 g/cm^3) and hardness (210 DPH) rubbing on the flats listed in Table 4. Conditions: 2.2 g load and 60 rpm in water.

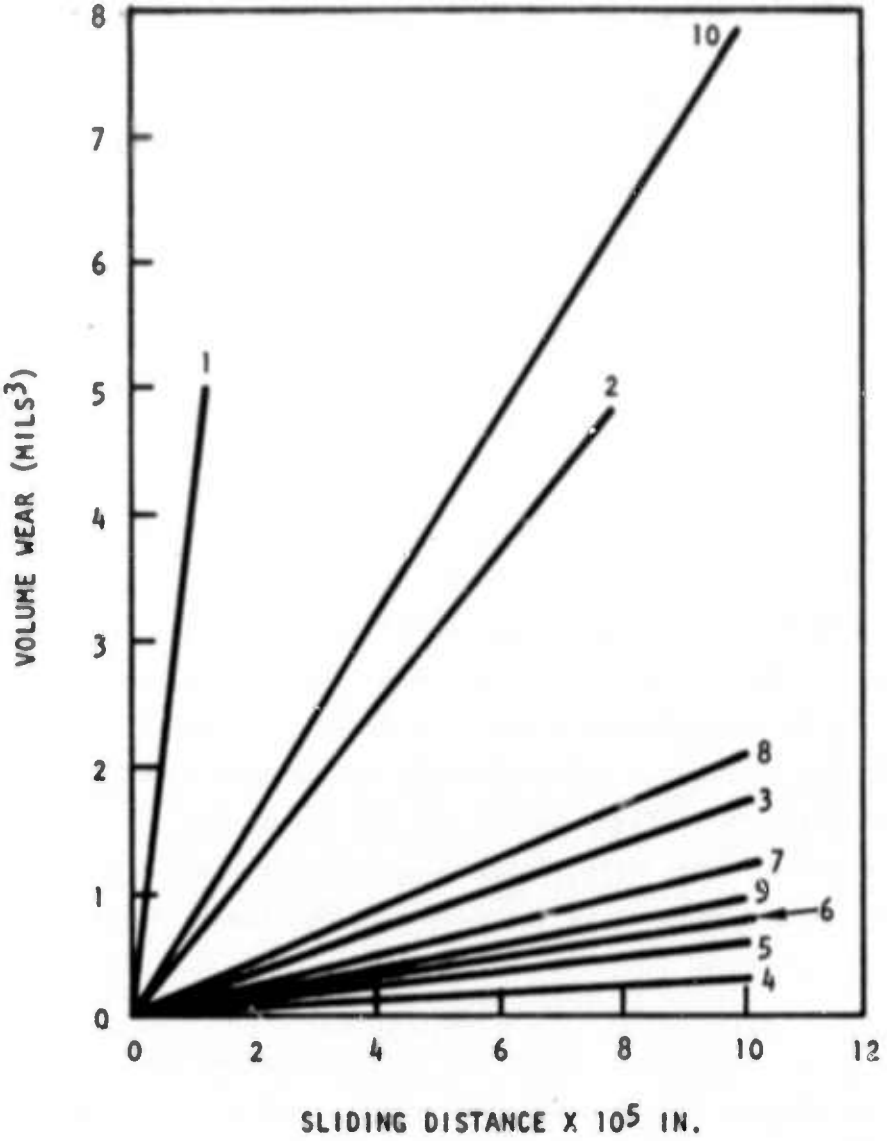

LC99166

Fig. 15. Wear caused by a pure carbon disk with a low density (1.46 g/cm^3) and hardness (153 DPH) rubbing on the flats listed in Table 4. Conditions: 2.2 g load and 60 rpm in water.

The data plotted in Figs. 13 through 15 for the case of pure carbon rubbing on various carbon flats are summarized in Fig. 16. The wear rates of pure carbon couples are strongly dependent on the hardness of both the flat and the disk. The rates drop steeply with hardness to a very low value at a DPH of approximately 210. In all cases the wear rates are very small when the carbon flat contains a silicon additive. The wear behavior can be expressed by two lines for a given disk with an intersection near 210 DPH. The abruptness of the change at 210 DPH suggests that different wear mechanisms may be involved when the flat contains silicon carbide particles in its microstructure.

5.2.2. Wear Caused by Silicon-Alloyed Carbon Disks Rubbing on Various Flats

Data relating wear caused by a silicon-alloyed disk containing 16 wt % silicon, with a carbon matrix density of 1.87 g/cm^3 and a hardness of 212 DPH (No. 6 in Table 4) rubbing on various flats are plotted in Fig. 17 as a function of sliding distance.* The relatively low hardness of the alloyed disk is due to the low carbon matrix density and high L_c value (Fig. 7 of Ref. 2). The wear rates for all the materials were lower than those for corresponding data in Figs. 13 through 15, except for the wear of the silicon-alloyed flats. The latter were higher by nearly an order of magnitude. The wear caused on titanium by silicon-alloyed carbon is particularly low.

The data for wear caused by the silicon-alloyed No. 6 (Table 4) disk rubbing on various pure and alloyed carbon flats are plotted in Fig. 18 as a function of the hardness of the flat. The data appear to fall on two separate lines, one for the pure carbon flats and one for the alloyed flats. For the pure carbon flats, the wear rate decreases as the hardness (and density) of the flat increases. The wear rates for the silicon-alloyed flats however are nearly constant. Pure carbon-silicon alloyed couples give minimal wear.

*Note that the data for this case that were reported in Fig. 23 of Ref. 2 were in error.

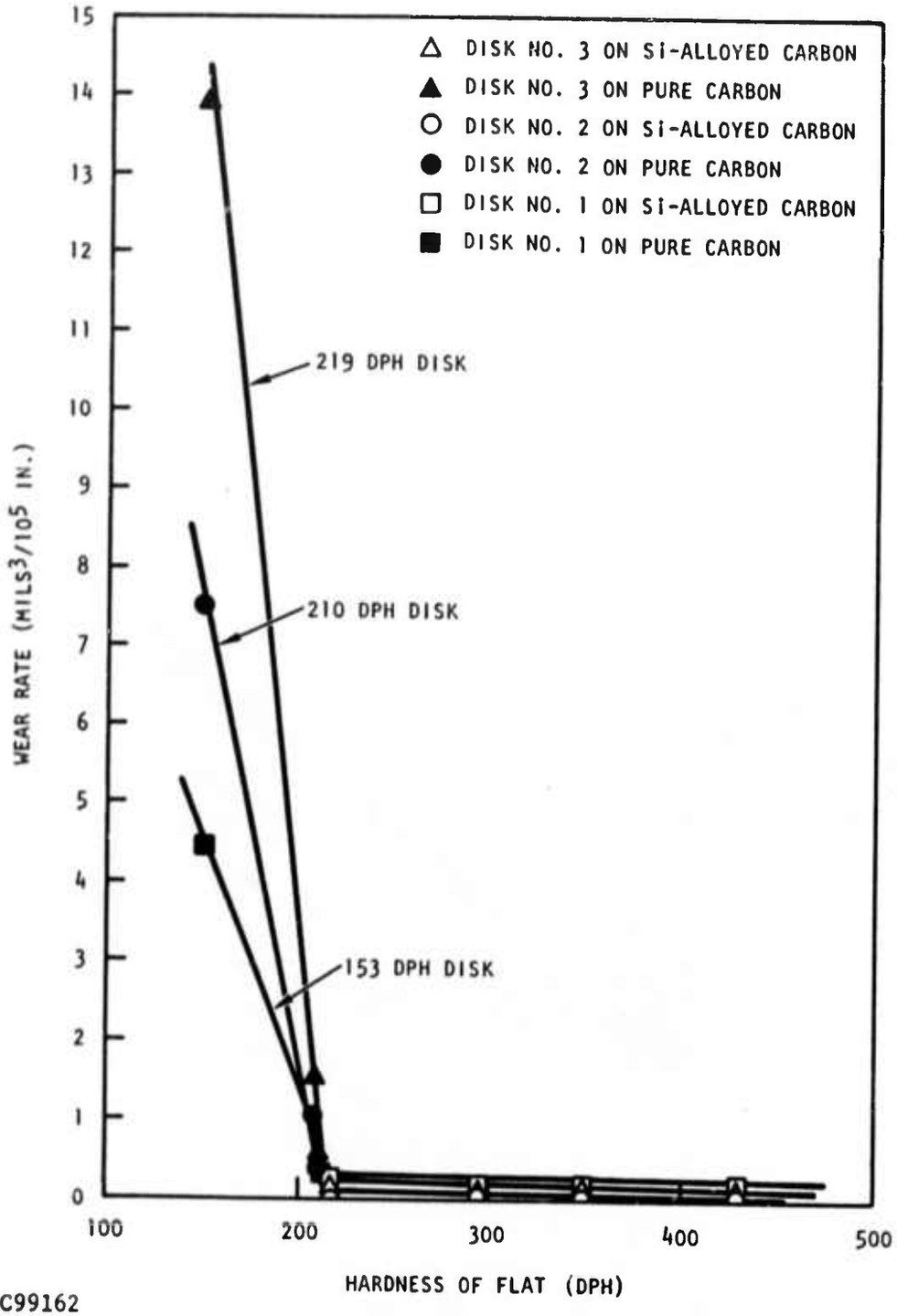

Fig. 16. Wear rates caused by various pure carbon disks rubbing on a variety of pure and alloyed carbon flats plotted as a function of the hardness of the flat. (Flats are identified in Table 4.) Conditions: 2.2 g load and 60 rpm in water.

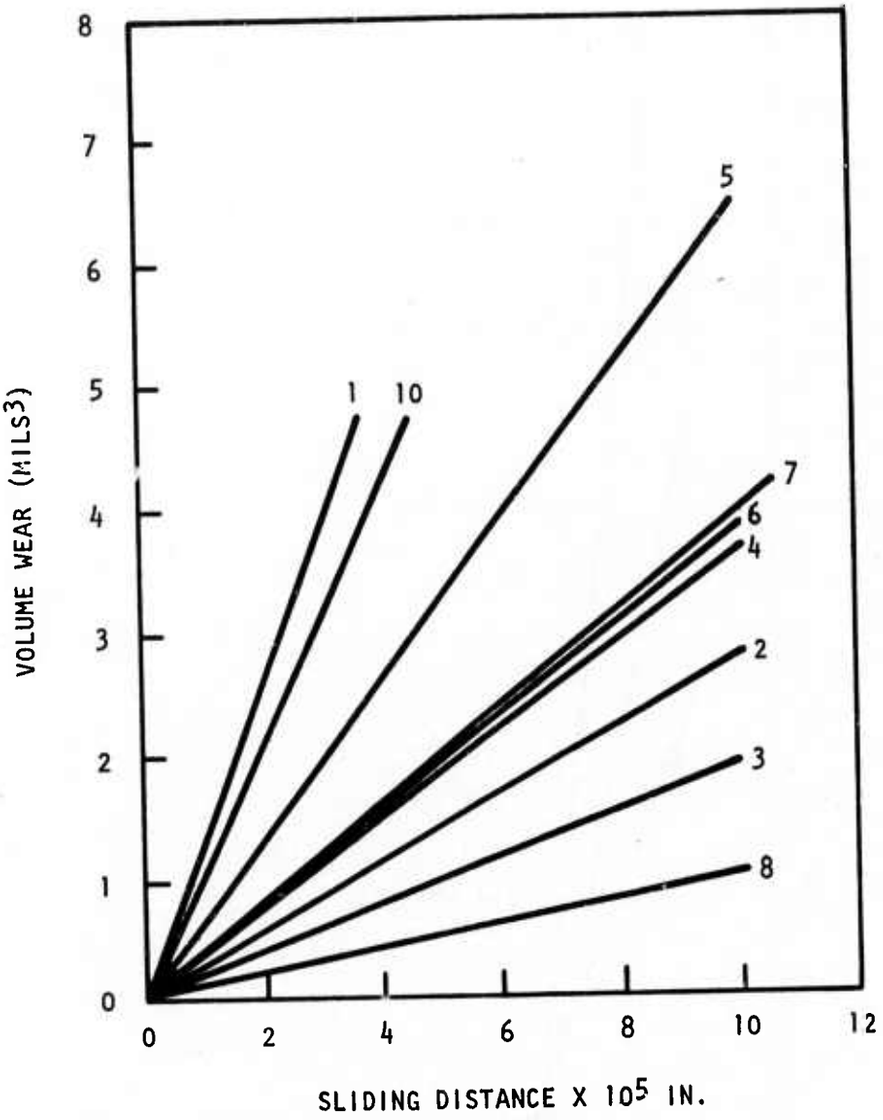

LC99167

Fig. 17. Wear caused by a silicon-alloyed (16 wt % Si) carbon disk with a carbon matrix density of 1.87 g/cm^3 and a hardness of 212 DPH rubbing on various flats. (Flats are identified in Table 4.) Conditions: 2.2 g load and 60 rpm in water.

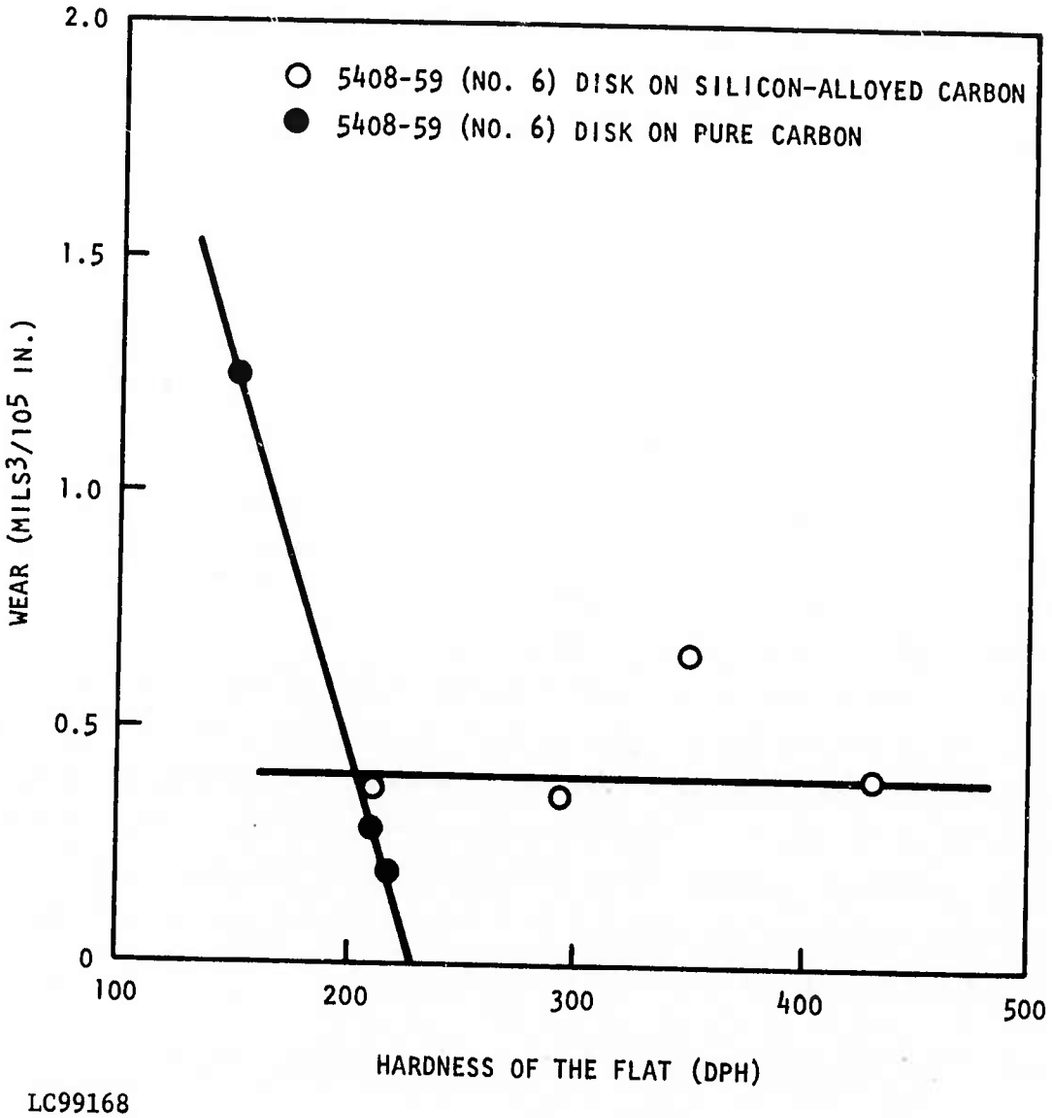

Fig. 18. Wear rates caused by a silicon-alloyed carbon disk (15 wt % Si, 1.87 g/cm^3 carbon matrix density, 212 DPH) rubbing on various carbon flats. Conditions: 2.2 g load and 60 rpm in water.

For nongalling materials, the wear resistance of a flat may be influenced by the magnitude of the elastic deformation that can occur at the contact points before microcracking occurs. If this is the case, the wear rate depends on the elastic energy that can be stored per unit volume, ε_e. The elastic energy that can be stored before fracture is proportional to the square of the elastic limit divided by twice the elastic modulus,

$$\varepsilon_e \propto \frac{\sigma f^2}{2E} \quad ,$$

so that a material with high strength and low modulus will presumably exhibit high wear resistance.

Kaae has shown that the strain energy to fracture rises with increasing density for the pure carbons deposited from propane so that the denser (and harder) pure carbons provide higher wear resistance (Ref. 3). Kaae and Gulden (Ref. 6) have further shown that the strain energy to fracture of the silicon-alloyed carbons is lower than that for the dense, pure carbons, and this may be the reason the alloyed flats are worn at a higher rate by an alloyed disk than are the dense, pure carbons. Accordingly, one would expect minimum wear of a carbon flat when the indenting surface (the disk) is soft and, for a given carbon disk, the wear is expected to be minimum when the elastic energy that can be stored in the carbon flat is maximum. Both dependencies are observed.

5.2.3. Wear Caused by Metal Disks Rubbing on Various Carbon Flats

The data that are available for wear caused by titanium disks rubbing on various carbon flats are plotted in Fig. 19.* The rates are high for the softer flats and decrease with increasing hardness of the flat. A set of incomplete data for Stellite 21 is presented in Fig. 20.

*Note that the wear caused by the titanium disk that was reported in Fig. 22 of Ref. 2 is erroneously high.

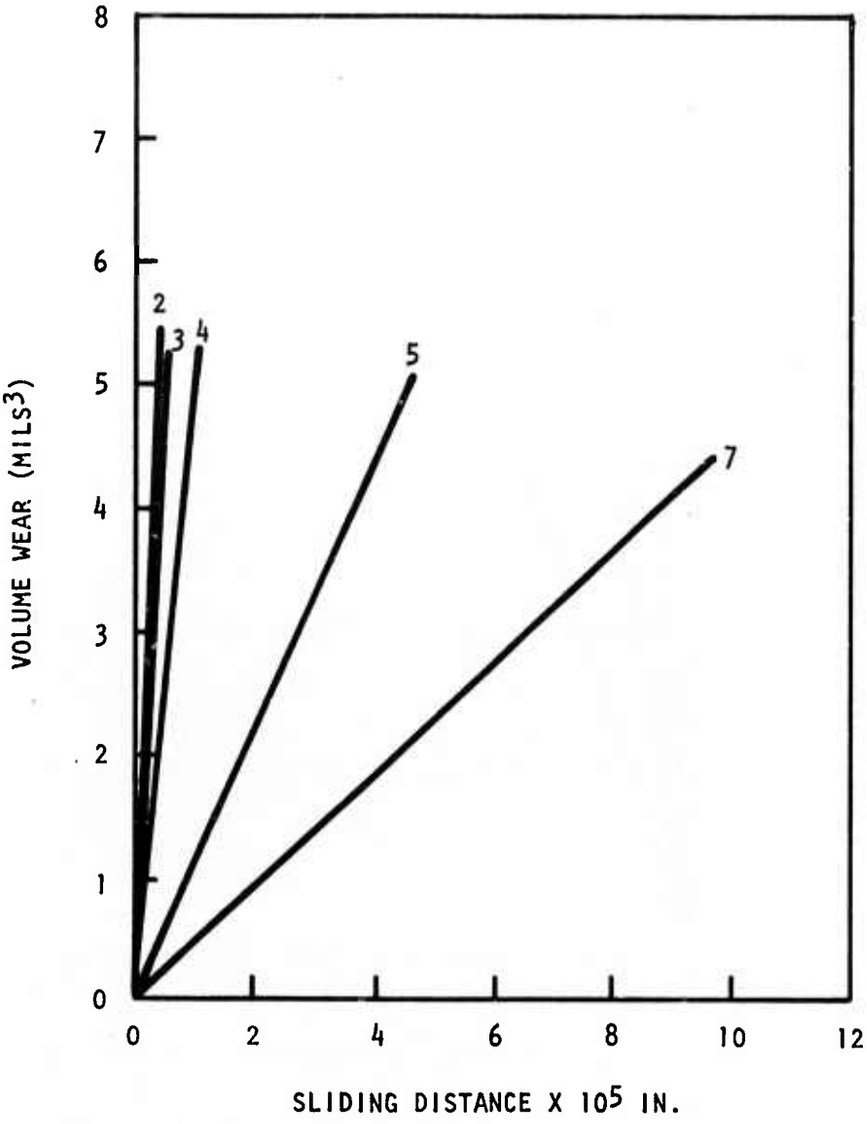

Fig. 19. Wear caused on various flats (see Table 4 for identification) by a pure titanium disk. Conditions: 2 g load and 60 rpm in water.

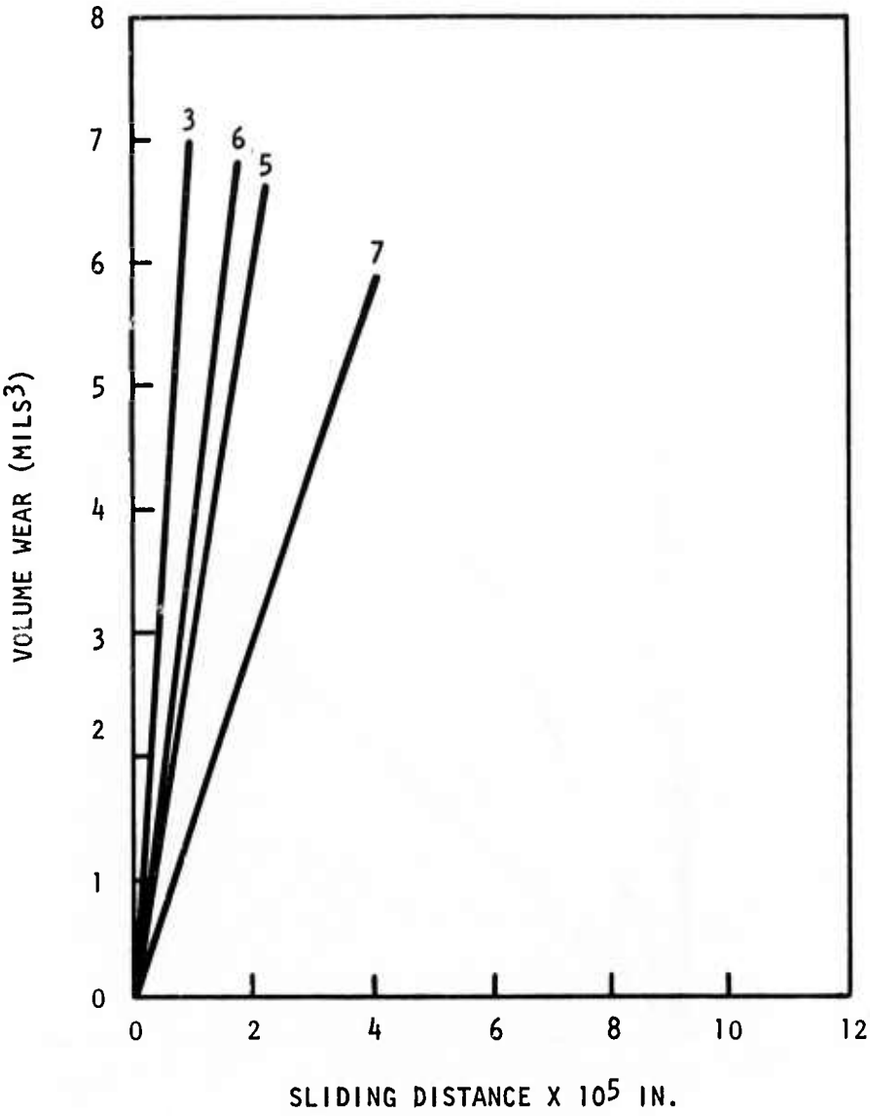

LC99170

Fig. 20. Wear caused on various flats (see Table 4) by a Stellite 21 disk. Conditions: 2 g load and 60 rpm in water.

The results of the wear studies will be presented at the 11th Conference on Carbon and submitted to Carbon for publication. The title of the paper will be "The Relationships Between the Wear Resistance of Isotropic Pyrolytic Carbons and Their Structure," by H. S. Shim, F. J. Schoen, and J. L. Kaae.

REFERENCES

1. Akins, R. J., et al., "Semiannual Technical Report for the Period 1 July 1971 to 31 December 1971, Carbon Research," Advanced Research Projects Agency Report Gulf-EL-A10968, Gulf Energy & Environmental Systems Company, January 31, 1972. AD-740 764
2. Akins, R. J., et al., "Semiannual Technical Report for the Period January 1, 1972 to June 30, 1972," Advanced Research Projects Agency Report Gulf-El-A12250, Gulf Energy & Environmental Systems Company, August 25, 1972. AD-748 223
3. Kaae, J. L., J. Nucl. Mater. 38, 42 (1971).
4. Kaae, J. L., Carbon 9, 291 (1971).
5. Kaae, J. L., J. Biomed. Mater. Res. 6, 279 (1972).
6. Kaae, J. L. and T. D. Gulden, J. Am. Ceram. Soc. 54, 606 (1971).
7. Bokros, J. C., Carbon 3, 201 (1965).
8. Ban, L. L., and W. M. Hess, "Microstructure of Carbons," paper presented at the Tenth Biennial Conference on Carbon, Bethlehem, Pa., June 1971.
9. Yokoyama, J., et al., Tanso 65, 44 (1971).
10. Tsuzuku, T., Carbon 1, 25 (1963).
11. Tsuzuku, T., Carbon 1, 511 (1964).
12. Leichter, H. L., and E. Robinson, J. Am. Ceram. Soc. 53, 197 (1970).
13. Barabanov, V. N., et al., Ind. Lab. 32, 459 (1964).